Journal of Peptide Science
J. Peptide Sci. **10**: 494–509 (2004)
Published online 2 February 2004 in Wiley InterScience (www.interscience.wiley.com). DOI: 10.1002/psc.559

JOURNAL OF PEPTIDE SCIENCE

The Relative Orientation of the Arg and Asp Side Chains Defined by a Pseudodihedral Angle as a Key Criterion for Evaluating the Structure–Activity Relationship of RGD Peptides

SARANTOS KOSTIDIS, ATHANASSIOS STAVRAKOUDIS, NIKOLAOS BIRIS, DEMOKRITOS TSOUKATOS, CONSTANTINOS SAKARELLOS and VASSILIOS TSIKARIS*

Department of Chemistry, University of Ioannina, Ioannina 45110, Greece

Received 1 October 2003
Accepted 19 November 2003

Abstract: The ability of an integrin to distinguish between the RGD-containing extracellular matrix proteins is thought to be due partially to the variety of RGD conformations. Three criteria have been proposed for the evaluation of the structure–activity relationship of RGD-containing peptides. These include: (i) the distance between the charged centres, (ii) the distance between the Arg C^{β} and Asp C^{β} atoms, and (iii) the pseudo-dihedral angle defining the Arg and Asp side-chain orientation formed by the Arg C^{ζ}, Arg C^{α}, Asp C^{α} and Asp C^{γ} atoms. A comparative conformation–activity study was performed between linear RGD peptides and strongly constrained cyclic (S,S) -CDC- bearing compounds, which cover a wide range of inhibition potency of platelet aggregation. It is concluded that the fulfilment of the $-45^{\circ} \leq$ pseudo-dihedral angle $\leq +45^{\circ}$ criterion is a prerequisite for an RGD compound to exhibit inhibitory activity. Once this criterion is accomplished, the longer the distance between the charged centres and/or between the Arg and Asp C^{β} atoms, the higher is the biological activity. In addition, the stronger the ionic interaction between Arg and Asp charged side chains, the lower the anti-aggregatory activity.

Keywords: integrin inhibitors; RGD conformation; RGD inhibitors; RGD SAR; RGD specificity; RGD structure–activity

INTRODUCTION

Integrins are the main cell surface receptors, mediating cell adhesion to extracellular matrices [1–3]. Of the known integrins, at least eight of them bind to the Arg-Gly-Asp (RGD) motif [3–5] as the primary recognition sequence of their ligands [6,7], such as fibronectin, vitronectin, osteopontin, collagen, thrombospondin, fibrinogen and von Willebrand factor, as well as to specific inhibitors of cell attachment, such as disintegrins [8]. Interactions between the RGD sequence and integrins are involved in many biological functions such as general cell adhesion [3], which influences migration, growth, differentiation and apoptosis of cells. Integrins also play a crucial role in platelet aggregation [9], inhibition of angiogenesis [10] and fertilization [11]. Modulation of platelet aggregation is of great significance in the treatment of thrombotic diseases [12]. Among the integrins GPIIb/IIIa is the main responsible membrane receptor for the aggregation phenomenon [13] via its binding to RGD-containing ligands such as fibrinogen [14], fibronectin [15,16], vitronectin [17] and von Willebrand factor [18]. In non-stimulated platelets GPIIb/IIIa is incapable of binding to most of its ligands [19], while under activation by several

* Correspondence to: Vassilios Tsikaris, Department of Chemistry, University of Ioannina, 45110 Ioannina, Greece;
e-mail: btsikari@cc.uoi.gr

agonists the receptor undergoes conformational changes [20–22] and consequently becomes able to interact with the proteins of the extracellular matrix. Fibrinogen binding to GPIIb/IIIa is mediated by two RGD-sites, RGDF (95–98) and RGDS (572–575), both located in the α-chain, as well as through the *C*-terminal dodecapeptide HHLGGAKQAGDV at the *C*-terminus of the γ-chain [23].

The wide range of functions by such a short amino acid sequence has been investigated by both structural and functional ways, in order to explore the relationship between structure and biological activity, as well as the specificity towards different receptors [5–7,24]. Structural studies of RGD-containing peptides and proteins [25–35] suggest that the RGD motif usually occurs at the apex of a solvent exposed loop [7,23,36], a characteristic of prime importance for its biological activity. However, different integrins distinguish small differences in the conformation and the sequential environment of various RGD sites in proteins with established RGD activity [24,37]. In various binding studies small RGD-containing peptides have been shown to compete successfully with the adhesive proteins [1,4,38,39]. The ability of an integrin to distinguish between different RGD-containing extracellular matrix proteins is partially due to the variety of RGD conformations. Linear and cyclic RGD-containing peptides have been studied by NMR and molecular dynamics simulations. A number of conformations including β-turns of types I, II or II′ for Arg-Gly and/or Gly-Asp sequences have been suggested [5,24,40–49]. In particular, emphasis has been given to the presence of a well defined Gly-Asp type II β-turn as a prerequisite for integrin binding, while selectivity of ligands has been correlated with the distances between either the C^{β} atoms [24,47–50] or the opposite charged centres of Arg and Asp residues [51]. On the other hand, it is not well understood how the residues flanking the RGD sequence affect the activity and selectivity of RGD peptides. These residues can be involved both in binding to the receptor [23,52] and in inducing a defined RGD conformation [53,54].

In a previous work on RGD peptides some very potent inhibitors of the human platelet aggregation ($IC_{50} = 1–10$ μM) were reported [55,56]. The IC_{50} values are 10–20 times lower in inhibiting the fibrinogen binding to activated human platelets (unpublished data). These compounds incorporate the cyclic motif (S,S) -CDC- and at least one positive charge. The cyclic scaffold induces a rather constrained orientation of the basic and acidic side chains. Structural studies indicated that the β-turn is not a prerequisite for their anti-aggregatory activity. On the contrary, a very good correlation between the pseudo-dihedral angle (*pdo*), which defines the relative orientation of the Arg and Asp side chains (formed by the Arg C^{ζ}, Arg C^{α}, Asp C^{α} and Asp C^{γ} atoms of the basic and acidic side chains) and activity was found ($-45^{\circ} \leq pdo \leq +45^{\circ}$). In the same study the presence of a second positive charge was estimated to enhance considerably the anti-aggregatory activity.

Stote [57] used the same pseudo-dihedral angle as an additional criterion for evaluating structure–activity relationship. A detailed analysis of the RGD sequence in protein structures was performed using the data set of crystal and NMR protein structures deposited in the Protein Data Bank. It was found that the region of pseudo-dihedral angle (*pdo*) is restricted between -150° and 90°. The interatomic distances between the Arg C^{β} and Asp C^{β} atoms and between the Arg C^{ζ} and Asp C^{γ} atoms were distributed in the range of 5.5–9 Å and 7.8–11.5 Å, respectively. By performing molecular dynamics simulations on the RGDW peptide, Bartels *et al.* [58] found that the distance between the C^{γ} atom of the Asp side chain and the C^{ζ} atom of the Arg side chain has an average value of 9.9 Å, with 11 Å being the most populated distance. The corresponding distance was proposed to be 10–15 Å in the case of decorsin, a potent 39-residue antagonist of GPIIb/IIIa receptor [33,35].

Recently, a detailed ^{1}H-NMR and molecular modelling analysis of Ac-RGD-NH_2 in DMSO-d_6 solution was reported [59]. It was demonstrated that this peptide, the shortest sequence that maintains an appreciable inhibitory activity ($IC_{50} \approx 500$ μM), adopts a very stable conformation in solution at room temperature which is stabilized by a hydrogen bonded ionic interaction between the Arg and Asp acid side chains. This interaction persists even at very high temperatures (>350 K). In this case the *pdo* values range between $-70^{\circ} \leq pdo \leq 0^{\circ}$.

The above mentioned data reveal that the pseudo-dihedral angle could possibly be utilized as a criterion for evaluating the structure–function relationship of RGD–containing peptides. Criteria such as the presence of a β-turn, the distance between Arg and Asp C^{β} atoms, the distance between the oppositely charged centres, and the presence of the ionic interaction could be envisaged as dependent upon the relative orientation of the side chains, which further correlates with the activity and selectivity

of an analogue. Furthermore, additional experimental data to estimate the contribution of the second positive charge to the conformational features and consequently to the biological activity are needed.

In this study, aimed at contributing to a better classification of the criteria concerning the structure–function relationship of RGD–containing peptides, the following compounds were designed, synthesized and studied: Ac-Ser-**Arg-Gly-Asp**-Val-Gly-**Arg**-Aib-Gly-Lys(Ac)-Aib-Gly-OH (**1**), Ac-Ser-**Arg-Gly-Asp**-Val-Gly-**Nle**-Aib-Gly-Lys(Ac)-Aib-Gly-OH (**2**), Ac-Ser-**Nle-Gly-Asp**-Val-Gly-**Arg**-Aib-Gly-Lys-(Ac)-Aib-Gly-OH (**3**) and Ac-**Arg-Aib-Gly-Asp**-Aib-Gly-**Arg**-Aib-Gly-Lys(Ac)-Aib-Gly-OH (**4**).

The *C*-terminal part of the analogues, which is known to exhibit helical preferences [60,61], was chosen in order to induce a regular secondary structure in the molecules, which could affect the relative orientation of the Arg and Asp side chains. Incorporation of an additional Arg residue will allow the evaluation of the role of a second positive charge. The size and primary structure of the designed peptides will also contribute to the assessment of the dominant forces of both the local conformation of the RGD motif and its flanking sequence.

A detailed conformational analysis was performed by ^{1}H NMR and molecular modelling calculations. The local conformation of the RGD motif and the role of the second positive charge are discussed and correlated with the anti-aggregatory potency of the analogues. A comparative conformation–activity analysis of the linear RGD peptides and some strongly constrained cyclic (S,S) -CDC- bearing compounds, which cover a wide range of inhibitory activity, is also presented.

MATERIALS AND METHODS

2-(1H-Benzotriazol-1-yl)-1,1,3,3-tetramethyluronium hexafluorophosphate (HBTU), 1-hydroxybenzotriazole (HOBt), *tert*-butoxycarbonyl (Boc) amino acids and 4-hydroxymethyl-phenylacetamidomethyl (PAM) resin were purchased from Neosystem Laboratoire (Strasbourg, France). Solvents were purchased from Labscan (Dublin, Ireland), while trifluoroacetic acid (TFA) and *N*,*N*-diisopropylethylamine (DIEA) were Merck-Schuchardt (Darmstadt, Germany) products. All reagents and solvents were used without further purification.

Peptide Synthesis

The synthesis of the peptides was carried out manually by a stepwise solid-phase procedure on a PAM resin following Boc chemistry [62]. Lysine was introduced as Boc-L-Lys(Fmoc)-OH (Fmoc: fluorenyl-γ-methoxycarbonyl), arginine as Boc-L-Arg(Tos)-OH (Tos: tosyl) and aspartic acid as Boc-L-Asp(OBzl)-OH (OBzl: benzyloxy). All coupling reactions were performed using a molar ratio of amino acid/HBTU/HOBt/DIEA/resin 3 : 3 : 3 : 9 : 1. The lysine side chain was deprotected by 20% piperidine in DMF, and acetylated using $(Ac)_2O$ (Ac: acetyl) in pyridine in an $(Ac)_2O$/resin 30 : 1 molar ratio. The Fmoc deprotection reaction of the Lys side chain was performed before the incorporation of the Asp residue in order to avoid aspartimide formation due to the basic conditions required. Acetylation was performed at the *N*-terminal amino group of compounds (**1**)–(**4**) after completion of the desired sequence. Cleavage from the resin was carried out using anhydrous hydrogen fluoride at -8° and $0\,^\circ$C for 30 and 90 min, respectively, in the presence of anisole and phenol as scavengers.

The crude peptides were purified by high performance liquid chromatography (HPLC; semi-preparative reverse phase C18 column) using gradient elution with the following solvents: A, H_2O/0.1% TFA and B, CH_3CN/0.1% TFA. The purity of the peptides was checked by analytical HPLC (analogue **1**: from 100% A to 70% A in 30 min, $R_t = 19.2$ min; analogue **2**: from 90% A to 60% A in 30 min, $R_t = 14.3$ min; analogue **3**: from 90% A to 60% A in 30 min, $R_t = 20.5$ min; analogue **4**: from 95% A to 60% A in 30 min, $R_t = 13.5$ min) and the correct molecular mass was confirmed by electrospray ionization–mass spectroscopy (ESI-MS) (analogue **1**:expected MW = 1242.36, found 1241.78; analogue **2**: expected MW = 1199.34, found 1198.43; analogue **3**: expected MW = 1199.34, found 1198.48; analogue **4**: expected MW = 1226.37, found 1225.63). Overall yields of the four analogues ranged from 19% to 51%.

Platelet Aggregation Assays

Fresh platelet rich plasma (PRP) was prepared from the whole blood of healthy volunteers by centrifugation at 160 **g** for 10 min at room temperature. Blood was anticoagulated with an aqueous solution based on sodium citrate (2.2%), citric acid (0.8%) and glucose (2.5%), (ACD). The remaining blood specimen was centrifuged at 3000 **g** for 20 min to prepare platelet poor plasma (PPP).

Assessment of the functional blockage of GPIIb/IIIa was made utilizing ADP-induced platelet aggregation in PRP. It was determined by the measured change in light transmission (PPP represents 100%), through the PRP (2.5×10^5 platelet/ml), on a Chrono-Log Model 500-Ca Lumi-Aggregometer, with stirring.

Aggregation was initiated by adding 10 μM ADP, the peptide analogues were added 1 min after in Tris-buffer saline (TBS) at pH 7.4, and the reaction was then allowed to proceed for a further 3 min. The inhibitory activity of the peptides in the ADP-induced platelet aggregation was measured and the IC_{50} value was determined as the concentration of the peptide required to produce 50% inhibition of the response to ADP.

^{1}H NMR Experiments

The NMR samples of compounds **1**–**4** were prepared by dissolving the solid material in H_2O and adjusting the pH to the desired value (~4.9) with NaOH or HCl. The aqueous solutions were lyophilized, and weighed amounts of the solid material were dissolved in DMSO-d_6 at concentrations of 5–8 mM. The 2D NMR experiments (COSY, TOCSY, NOESY) were performed at 300 K, while 1D NMR experiments were carried out in the range from 300 to 350 K. All spectra were recorded on a Bruker AMX 400 spectrometer. Standard pulse sequences were applied for the homonuclear two-dimensional COSY, TOCSY and NOESY experiments. The TOCSY and NOESY spectra were obtained using a mixing time of 100 ms and 350 ms, respectively. NMR data were processed and analysed using WINNMR software.

Structure Calculations

Structure calculations were carried out using DYANA software [63]. The distance restraints used as inputs in DYANA were derived from the ^{1}H-^{1}H NOESY spectra of the peptides reconstituted in DMSO-d_6 after lyophilization from an aqueous solution at pH 4.9. Upper-limit cross-peak intensities were classified as strong (up to 2.8 Å), medium (up to 3.5 Å) and weak (up to 5 Å) and were used as input restraints for the calculations. Appropriate corrections for centre averaging were added to DYANA restraints for degenerate proton resonances [64]. No lower limits were used. Constraints for hydrogen bonds were added when appearing in at least in 6 out of 20 best structures in preliminary structure calculations, and the incorporation of the related restraints did not lead to any other distance or dihedral angle violation. Hydrogen bonds were assumed to exist when the distance between the hydrogen and acceptor atoms was less than 2.5 Å and the angle donor-hydrogen-acceptor was larger than 120°. $^3J_{\alpha\beta}$ and $^3J_{N\alpha}$ coupling constants were included with the default tolerance of 2.0 Hz. To all distance and dihedral angle constraints were assigned the default relative weight of 1. Constraints for φ, ψ and χ^1 torsion angles were calculated using the HABAS program of DYANA package. The default tolerance of 0.05 at target function units was applied. The calculations were performed using the standard minimization protocol and the REDAC strategy implemented in DYANA. After a first run of REDAC, without hydrogen bonding restraints, calculated hydrogen bonds, present in at least 7 out of the 20 best resulting structures, were inserted as additional restraints to new REDAC runs. These restraints were taken into consideration for further REDAC runs if they had no impact to other (experimentally determined) initial restraints. The procedure was repeated until no other restraints came out. For each peptide, 100 structures were generated and a bundle of 20 DYANA conformers with the smallest residual target function values was used as the basis for the representation of peptide conformation in solution. Clustering of the 20 best conformers was performed based on the superposition of the backbone atoms, excluding the *N*- and *C*-terminal cap residues. Two conformers were assigned to be members of the same family when they fitted with a RMSD less than 1 Å. The most populated family constituted the first cluster, and its members were removed from the set. The fitting procedure was repeated from the beginning until there was no conformer in the initial set. The program MOLMOL [65] was used for structure representation and analysis.

RESULTS AND DISCUSSION

All of the proton resonances of the four analogues were assigned by combining 2D ^{1}H-^{1}H COSY, TOCSY and NOESY spectra. The information deduced from these experiments was interpreted in terms of both local (RGD motif) and global (the overall peptide backbone) conformational features. A detailed evaluation and comparison of the behaviour of Arg and Asp side chains, either in all of the analogues or in each one at various temperatures, pointed out significant conformational differences, which were correlated to their biological activities.

^{1}H NMR Conformational Analysis of Analogue 1

Figure 1 shows the detected NOEs of peptide **1** in DMSO-d_6 solution. Medium-range NOEs of types d_{NN} $(i, i+2)$ (G9 H^N/Aib11 H^N, K10 H^N/G12 H^N) and $d_{\alpha N}$ $(i, i+2)$ (D4 H^{α}/G6 H^N, G6 $H^{\alpha/\alpha'}$/Aib8 H^N, R7 H^{α}/G9 H^N and K10 H^{α}/G12 H^N) were detected, especially for the *C*-terminal part of the analogue. Types d_{NN} $(i, i+2)$ and $d_{\alpha N}$ $(i, i+2)$ NOEs could originate either from a local 'helix type' or from β-turn structures, located at the *C*-terminal part of the peptide. This conclusion was further supported by the low absolute temperature coefficient values observed for the K10 H^N, Aib11 H^N and G12 H^N amide protons (Table 1). These values suggest either their participation in hydrogen bonds or their protection from solvent accessibility. Interestingly, in the *N*-terminal segment of the peptide medium-range NOEs for the backbone protons were not observed. In addition, high absolute temperature coefficient values were determined for almost all of the backbone amide protons of this segment, except for V5 H^N which showed a positive value. Despite this observation, the positive temperature coefficient value of V5 H^N (Table 1), the presence of R2 $H^{\beta/\beta'}$/D4 H^N and V5 H^N/R7 $H^{\beta/\beta'}$ NOEs (Figure 1) and the Arg and Asp side chains behaviour, suggest that a particular folding occurs in the sequence -R^2GDVGR^7-. The strong downfield shifts of both the R2 and R7 H^{ε} guanidinium protons indicates that they are involved in hydrogen bonding [59,66,67] (Figure 2). The high linewidth ($\Delta\nu_{1/2}$) values at 300 K (70 and 78 Hz for R2 and R7 H^{ε}, respectively; Figure 3) and their temperature dependence indicate that these protons participate in an exchange process, which becomes very fast at 350 K. This exchange process may involve the hydrogen bonded and the free state, in agreement with literature data [59]. The variation of the linewidths of the R2 and R7 H^{η} protons upon increase of the temperature was opposite to that observed for the H^{ε} protons. Thus, an initial broadening of the resonances up to 320 K was observed followed by a strong sharpening at higher temperatures. This behaviour of the R2,7 H^{η} protons compared with that observed in the case for either Ac-RGD-NH_2 or analogue **2** (see below; Figure 4) is compatible with their non-hydrogen bonded state [59]. Taking into consideration the fact that the R2 $H^{\beta/\beta'}$ and the R7 $H^{\beta/\beta'}$ protons showed NOEs with the D4 H^N and the V5 H^N protons, respectively, it can be envisaged that both Arg side chains move toward the central part of this peptide segment, probably targeting the Asp side chain. This hypothesis was also supported by the D4 $^3J_{\alpha\beta}$ and $^3J_{\alpha\beta'}$ coupling constant values (3.7 and 5.1 Hz, respectively). The reduced values indicate the presence of a high percentage (~65%; Table 2) of the g^+ ($\chi^1 \approx 60^\circ$) rotational state about

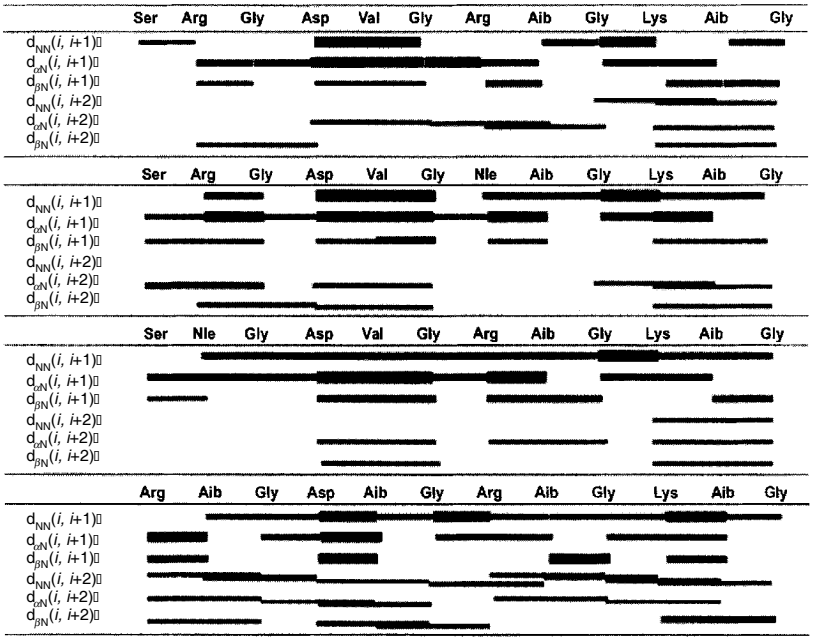

Figure 1 NOEs detected for analogues **1–4** in DMSO-d_6 solution (TE = 300 K and mixing time t_m = 350 ms).

Table 1 Temperature Coefficient ($\Delta\delta/\Delta T$, ppm/K) and Coupling Constant ($^3J_{\alpha N}$, Hz) Values for Analogues **1–4** in DMSO-d_6 Solution

Analogue 1	Ser	Arg	Gly	Asp	Val	Gly	Arg	Aib	Gly	Lys (Ac)	Aib	Gly
$(\Delta\delta/\Delta T) \times 10^3$	−4.5	−4.9	−5.6	−4.4	+2.0	−4.0	−4.3	−6.4	−3.7	−2.0	−2.6	−0.9
$^3J_{\alpha N}$ (Hz)	7.52	6.64	6.61/ 4.01	7.52	7.96	4.84/ 5.32	7.52		4.61/ 6.17	8.4		
Analogue 2	Ser	Arg	Gly	Asp	Val	Gly	Nle	Aib	Gly	Lys (Ac)	Aib	Gly
$(\Delta\delta/\Delta T) \times 10^3$	−5.2	−5.1	−4.3	−1.0	−0.2	−5.0	−3.6	−7.7	−3.6	−1.7	−4.2	−1.7
$^3J_{\alpha N}$ (Hz)	7.96	7.96	6.63/ 4.90	7.96	7.96	4.97/ 6.75			6.71/ 4.81	7.48		
Analogue 3	Ser	Nle	Gly	Asp	Val	Gly	Arg	Aib	Gly	Lys (Ac)	Aib	Gly
$(\Delta\delta/\Delta T) \times 10^3$	−5.3	−5.2	−4.1	−3.7	−5.5	−3.2	−1.8	−5.6	−4.3	−1.6	−2.7	−0.3
$^3J_{\alpha N}$ (Hz)	7.96	7.96		7.08	4.84		5.32			8.40		4.28
Analogue 4	Arg	Aib	Gly	Asp	Aib	Gly	Arg	Aib	Gly	Lys (Ac)	Aib	Gly
$(\Delta\delta/\Delta T) \times 10^3$	−8.4	−8.0	−3.7	0.0	−2.7	−1.7	−1.1	−1.7	−2.1	−5.2	−1.7	−0.3
$^3J_{\alpha N}$ (Hz)	8.08		6.20/ 5.76	7.72		4.88/ 4.88	5.52		6.13/ 6.03	5.52		4.00/ 4.08

the C^{α}–C^{β} bond, which is the least energetically favoured rotamer under free rotational conditions [68,69]. Conformational restrictions are probably responsible for this unfavoured arrangement of the Asp side chain. The equilibrium of the hypothesized dual interaction of the Asp side chain seems to be shifted toward R2 H^{ε}. This conclusion was obtained by comparing the chemical shift differences ($\Delta\delta$) of the geminal side-chain aliphatic protons of R2 and R7 (Table 2). The proposed interactions induce a local specific folding and rigidification of the peptide backbone (for example, compare $\Delta\delta$ of G3 $H^{\alpha\alpha'}$ of analogues **1** and **3**; Table 2), which could explain the protection of the V5 H^N from the solvent (positive temperature coefficient value, 2×10^{-3} ppm/K).

^{1}H NMR Conformational Analysis of Analogues 2 and 3

The sequence of analogue **2** is almost identical to **1**, with a single substitution of Nle7 for Arg7. Despite this single substitution, appreciable changes were induced in the peptide conformation. The most affected parts of the molecule were the R2 guanidinium group and the Asp side chain as indicated by the following observations: (i) a considerable downfield shift (δR2 $H^{\varepsilon} \approx 10.1$ ppm) and sharpening of the R2 H^{ε} resonance (Figure 3); (ii) a complete alteration of the behaviour of the R2 H^{η} protons upon heating (a relatively sharp peak corresponding to only two protons was detected at 300 K, which progressively broadened and could not be detected even at 350 K (Figure 4); and (iii) an increase of $\Delta\delta$ of the D4 $H^{\beta\beta'}$ geminal protons (0.41 ppm compared with 0.28 ppm for analogue **1**; Table 2). The conformational behaviour of the -R^2GDV^5- segment is almost identical to that observed in the case of Ac-RGD-NH_2, for which a detailed analysis was recently presented [59]. In the latter peptide an ionic interaction between Arg and Asp side chains, which is stabilized by two hydrogen-bonded interactions involving R H^{ε} and one R H^{η} protons, was proposed. The same conclusion seems to hold true for analogue **2** and was further supported by the ^{1}H NMR results of analogue **3**. Thus, since the proposed interaction in analogue **2** between R2 and D4 side chains cannot exist in the case of analogue **3** (Nle2 has

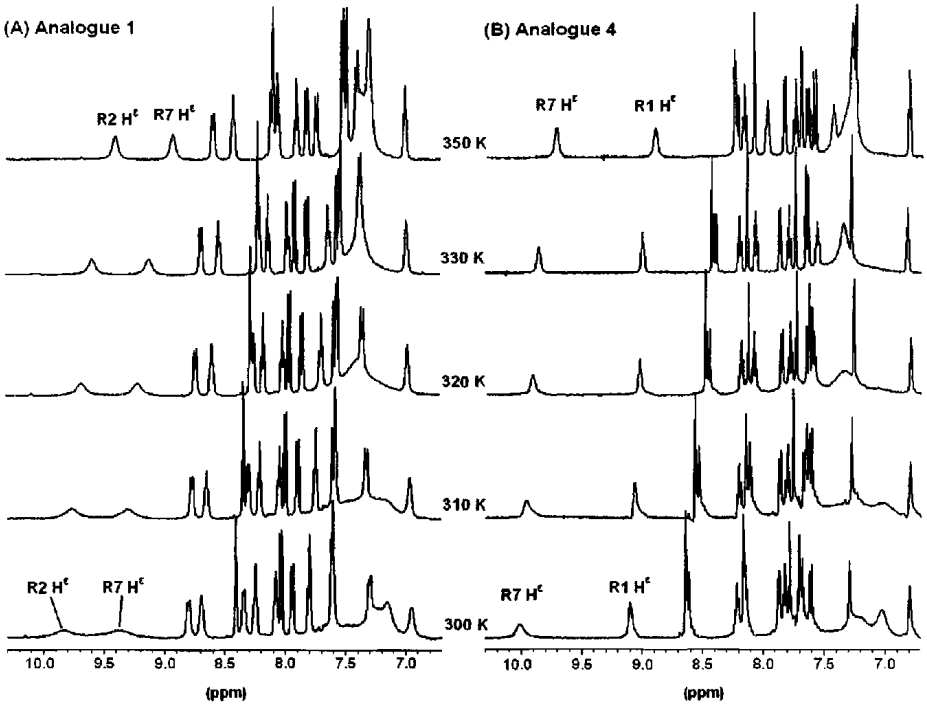

Figure 2 H^N region of the 400 MHz ^1H NMR spectra in DMSO-d_6 solution of analogues **1** (**A**) and **4** (**B**) at various temperatures.

replaced R2), significant differences were expected for this part of the molecule. Indeed, the $\Delta\delta$ chemical shift difference of the D4 $H^{\beta\beta'}$ geminal protons is considerably reduced in the case of analogue **3** (0.07 ppm for **3** instead of 0.47 ppm for **2**; Table 2) indicating a free rotational state of this side chain. In agreement with this finding, the estimated percentage for the D4 C^{α}-C^{β} g^+ rotamer ($\chi^1 = +60^\circ$) is also considerably reduced (23% for **3** instead of 69% for **2**; Table 2). Not only the flexibility of the D4 side chain but also of the flanking part of the peptide backbone was clearly evidenced by comparing the chemical shift differences between the G3 $H^{\alpha\alpha'}$ protons of analogues **3** ($\Delta\delta \approx 0.05$ ppm) and **2** ($\Delta\delta \approx 0.54$ ppm). Moreover, the temperature coefficient values for D4 H^N and V5 H^N protons (-3.7×10^{-3} and -5.5×10^{-3} ppm/K, respectively; Table 1) in the case of analogue **3** confirmed that these amide protons are exposed to the solvent. These data indicate that in the case of analogue **3** the absence of an ionic interaction results in a higher local flexibility of the peptide backbone and Asp side chain. However, the *C*-terminal part of the two molecules seems to possess similar conformations, as it was evaluated from the observed NOEs (Figure 1) and the amide proton temperature coefficient values (Table 1).

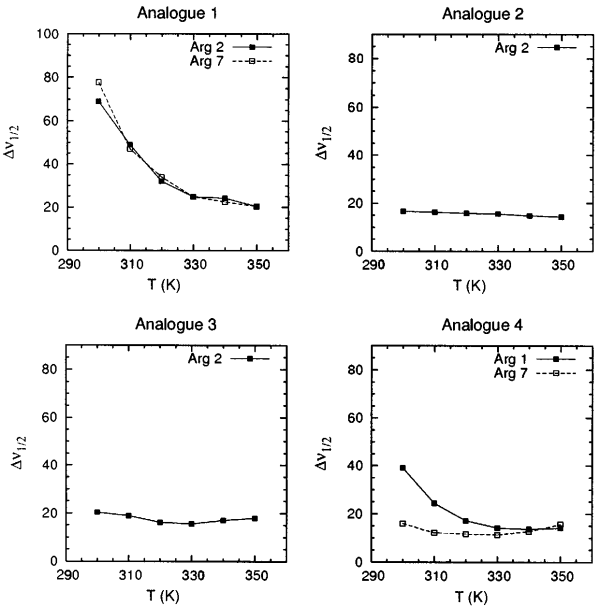

Figure 3 Temperature-dependent variations of the linewidths ($\Delta\upsilon_{1/2}$) of the R1(2) and R7 H^{ε} proton resonances in DMSO-d_6 solution for analogues **1–4**.

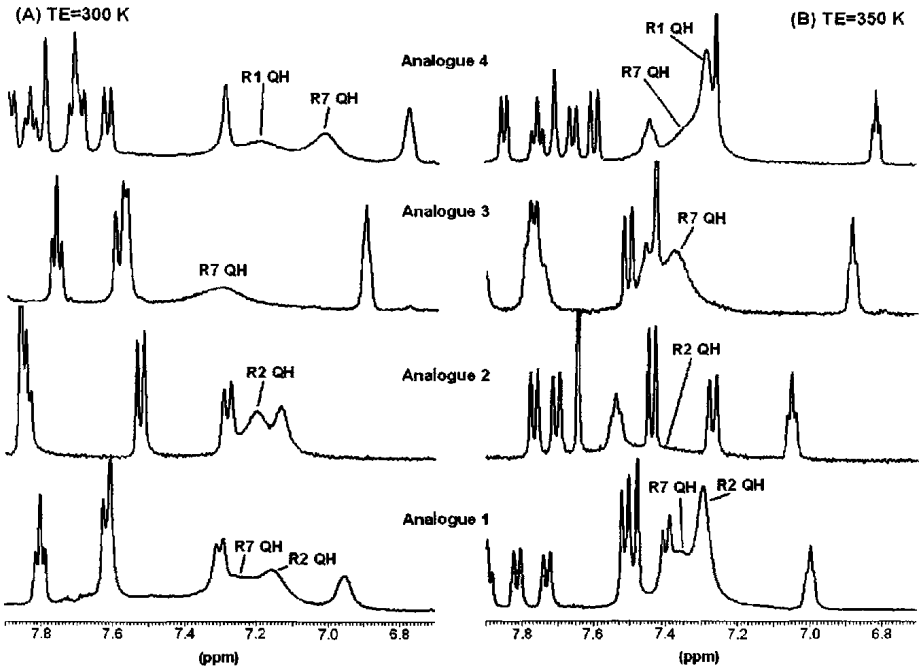

Figure 4 H^N region of the 400 MHz ^1H NMR spectra in DMSO-d_6 solution for analogues **1–4** at 300 K (**A**) and 350 K (**B**), respectively. All Arg H^N protons are presented as pseudoatoms (QH) according to reference [71].

Table 2 Chemical Shift Differences ($\Delta\delta$, ppm) for the R1(2), D4, G3 and G6 Geminal Protons and Distribution of the D4 C^α-C^β Rotamers for Analogues **1–4** in DMSO-d_6 Solution

Analogue	$\Delta\delta$ (ppm)					D^4 C^α-C^β rotamers[a]		
	$R^{1(2)}/R^7$ $H^{\beta\beta'}$	$R^{1(2)}/R^7$ $H^{\gamma\gamma'}$	$R^{1(2)}/R^7$ $H^{\delta\delta'}$	G^3/G^6 $H^{\alpha\alpha'}$	D^4 $H^{\beta\beta'}$	I (%)	II (%)	III (%)
1	0.35/0.13	0.07/0.15	0.23/0.00	0.47/0.05	0.28	8	27	65
2	0.37/*SR*[b]	0.07/*SR*	0.17/*SR*	0.54/0.07	0.41	9	22	69
3	*SR*/0.19	*SR*/0.00	*SR*/0.09	0.05/0.12	0.07	51	26	23
4	0.15/0.21	0.0/0.00	0.06/0.00	0.28/0.11	0.30	45	18	37

[a] Rotamer I ($\chi^1 = -60°$), II ($\chi^1 = 180°$), III ($\chi^1 = 60°$). The values of J_g and J_t used for estimation of the rotamer populations were 2.32 and 13.70 Hz, respectively.
[b] *SR*: substituted residue (Nle for Arg).

^{1}H NMR Conformational Analysis of Analogue 4

As expected, analogue **4**, due to the high content of Aib, adopts a 3_{10}-helical structure. This conclusion was obtained from the observed d_{NN} $(i, i+2)$ and $d_{\alpha N}$ $(i, i+2)$ NOEs along the whole peptide backbone (Figure 1). In a very good agreement, the temperature coefficient values for all of the backbone amide protons within the sequence, -D^4AibGRAibGK(Ac)AibG^{12}, indicate that these protons are protected from the solvent and probably involved in hydrogen bonding (Table 1). Further support for the helical structure of analogue **4** was given by the low values of the $^3J_{\alpha N}$ coupling constants, measured from the 1 D high-resolution spectrum (Table 1). Evidence for the proximity of the R1 and R7 side chains to the Asp residue was provided by the observed NOEs ($D4$ $H^{\beta\beta'}$/R7 H^N, R1 H^ε/D4 $H^{\beta\beta'}$, R1 H^ε/D4 H^N, R1 $H^{\beta\beta'}$/D4 H^N; Figure 1). In this case, the R7 H^ε proton interaction with the Asp β-carboxylate group is probably stronger than that of R1 H^ε ($\delta \approx 10.05$ and 9.12 ppm for R7 H^ε and R1 H^ε, respectively). In agreement with this finding, the

temperature dependence of the linewidth of R7 H^{ε} revealed that this proton participates in a slower exchange process than the R1 H^{ε} proton, probably between an hydrogen-bonded and an open-state (Figures 2 and 3). The strength of both R1 H^{ε} and R7 H^{ε} interactions, however, is probably quite weak, as it can be estimated from the behaviour of the aliphatic part of both Arg side chains (small chemical shift differences between the geminal protons; Table 2).

Structure Calculations for Peptide 1

DYANA calculations on peptide 1 produced a set of conformations with a relatively low target function (Table 3). Twenty structures with the lowest energy were selected for further analysis. In the selected structures the backbone atoms fit with RMSD of 0.867 Å (residues 2–11), and no dihedral angle or distance restraint violations (longer than 0.3 Å) were observed. The peptide does not exhibit any overall regular secondary structure, although five intramolecular hydrogen bonds are present (R2 O . . . V5 H^N, G6 O . . . Aib8 H^N, Aib8 O . . . Aib11 H^N, G9 O . . . Aib11 H^N, K10 O . . . G12 H^N), resulting in 'local' helix-type conformation. Although hydrogen-bonded interactions between the polar side chains of the Arg and Asp residues were not observed, electrostatic interactions were identified: R2 C^{ζ}-D4 C^{γ} and R7 C^{ζ}-D4 C^{γ} with average distances ~6 Å, and 6.5 Å, respectively. The Asp side chain lies between the two Arg residues, but it shows a preference for parallel orientation with the side chain of R2 and perpendicular orientation with the side chain of R7. The two Arg side chains lie in almost opposite directions, as the pseudo-dihedral angle defined by the R2 (R1) C^{ζ}, R^2 (R1) C^{α}, R7 C^{α}, R7 C^{ζ} (*pdorr*)

Table 3 Summary of Conformational Constraints and Statistics for the 10 Best Structures of Analogues **1–4**

Constraint classification	Analogue			
	1	**2**	**3**	**4**
Total number of NOEs	95	85	93	93
Number of backbone–backbone NOEs	42	40	49	45
Number of backbone–side chain NOEs	45	41	39	44
Number of side chain–side chain NOEs	8	4	5	4
Number of intraresidue NOEs	41	41	39	39
Number of interresidue NOEs	54	44	54	54
Number strong NOEs (≤2.8 Å)	15	9	3	17
Number medium NOEs (≤3.5 Å)	37	43	44	43
Number weak NOEs (≤5.0 Å)	43	33	46	33
Number of J	14	13	10	10
Number of $^3J_{N\alpha}$	12	13	8	8
Number of $^3J_{\alpha\beta}$	2	0	2	2
Number of hydrogen bonds	5	0	0	5
Calculation results				
Number of structure calculated	100	100	100	100
Number of final structures	20	20	20	20
Min/max target function of final structures	1.01/1.03	1.38/4.12	3.20/13.26	1.74/1.95
Number of distance restraint violations >0.3 Å	0	1	12	0
Number of distance restraint violations >0.2 Å	0	2	12	0
Number of torsion angle violations	0	0	0	0
Mean global heavy atom RMSD	2.71	5.65	4.76	3.59
Mean global backbone RMSD	1.56	4.50	3.30	2.48
Mean global backbone RMSD (residues 2–11)	0.867	—	—	1.459

values spread around -150°. The above results concerning the behaviour of the charged side chains are in very good agreement with the NMR findings, although no related constraints were used as inputs in DYANA calculations. The *N*-terminal part of analogue **1** (residues 2 to 7) has an RMSD value of 0.179 Å, suggesting a very stable local conformation. The hydrogen bond between R2 carbonyl oxygen and V5 amide proton stabilizes a type I β-turn, in agreement with the low temperature coefficient value of V5 H^N estimated from the NMR experiments. A very low RMSD value (0.119 Å) was also obtained for the *C*-terminal part (residues 9 to 12) of the molecule. Interestingly, the values of the Aib8 ψ angle are either concentrated at $-52.4^{\circ} \pm 0.1^{\circ}$, or at $-66.2^{\circ} \pm 3.4^{\circ}$, resulting in two clusters in the *C*-terminal part (Figure 5). This behaviour of the Aib8 may arise from the conformational exchange induced by the interactions between the D4 and R2/R7 charged side chains, as also evidenced by the NMR findings.

Structure Calculations for Peptides 2 and 3

DYANA calculations did not result in structures free of violations for analogues **2** and **3** (Table 3). This finding probably arises from the fact that the NMR-derived backbone restraints are considerably fewer compared with the other two analogues. It is worth noting that the analogues have no regular secondary structure nor hydrogen bond stabilization was observed, contrary to the other two analogues. Consequently, a clear orientation of the charged side chains was not seen. It seems that the substitution of Arg by Nle dramatically destabilizes the secondary structure, leading to the loss of biological activity.

Structure Calculations for Peptide 4

The backbone atoms of the 20 lowest energy selected structures of peptide **4** fit with RMSD of 1.459 Å (residues 2–11), and no dihedral angle or distance restraint violations larger than 0.3 Å, were observed (Table 3). A 3_{10}-helical conformation (from residue 4 to residue 12), stabilized by five backbone hydrogen bonds (D4 O...Arg7 H^N, Aib5 O...Aib8 H^N, Arg7 O...K10 H^N, Aib8 O...Aib11 H^N, K10 O...G12 H^N), was found for this peptide in good agreement with the NMR results. Interactions between the Arg and Asp side chains take place through electrostatic forces, without hydrogen bonding, as in peptide **1**. The R2 C^{ζ}-D4 C^{γ} and R7 C^{ζ}-D4 C^{γ} average distances were found ~6.3 Å, and 6.5 Å, respectively. Unlike

Figure 5 Overlay of the backbone atoms (segment 2–11) of the 20 best structures for analogue **1**. The two clusters are represented as cylinders of variable radius according to RMSD from the mean structure. The orientations of the R2, D4 and R7 side chains are also depicted.

peptide **1**, a clear-cut orientation of Asp side chain towards the two Arg side chains was not seen (Figure 6).

Structure – Activity Relationship

The IC_{50} values of all the analogues studied, as well as of those used for comparison, are given in Table 4. Incorporation of the RGD sequence in analogue **1** resulted in a two-fold increase of the anti-aggregatory activity compared with Ac-RGD-NH_2.

Table 4 Anti-aggregatory Activity of the Analogues Examined

Peptide analogues	Inhibition of human platelet aggregation IC_{50} (μM)
Ac-SRGDVGRAibGK(Ac)AibG (**1**)	219
Ac-SRGDVGNleAibGK(Ac)AibG (**2**)	2000
Ac-SNleGDVGRAibGK(Ac)AibG (**3**)	>2000
Ac-RAibGDAibGRAibGK(Ac)AibG (**4**)	>2000
(S,S) Ac RCDCR-NH_2	4.3[a]
(S,S) PRCDCK-NH_2	10.6[a]
(S,S) Ac-RCDC-NH_2	105[a]
Ac-RGD-NH_2	~500[a]

[a] From reference [55].

Surprisingly, substitution of the second positive charge (Nle for R7) in analogue **2**, led to loss of activity. This result highlights the significant contribution of the second positive charge to the biological activity of the analogue, and it is in very good agreement with the previously reported data concerning the (S,S) Ac-RCDC-NH_2 and (S,S) Ac-RCDCR-NH_2 compounds [55]. In this latter case removal of the second positive charge resulted in a 20-fold less active analogue (Table 4). The validity of three structural criteria was examined to gain further insight into the structure–activity relationship. Figure 7A depicts the distance distribution between the C^{ζ} atom of R2 (R1) and the C^{γ} atom of D4 selected from the ten best DYANA structures of analogues **1**, **2**, and **4**. It is evident that no correlation can be deduced concerning the distance of the charged centres and the biological activity. The same conclusion results from the evaluation of the distance between the C^{β} atoms of R2 (R1) and D4 residues (Figure 7B). The differences between active and non-active compounds become more evident when the *pdo* values are compared (Figure 7C). Thus, the active analogue **1** fits considerably well into the proposed *pdo* range ($-45^{\circ} \leq pdo \leq +45^{\circ}$), while the same pseudo-dihedral angle of the non-active peptides **2** and **4** ranges between -180° to $+180^{\circ}$. Based on these results, it was

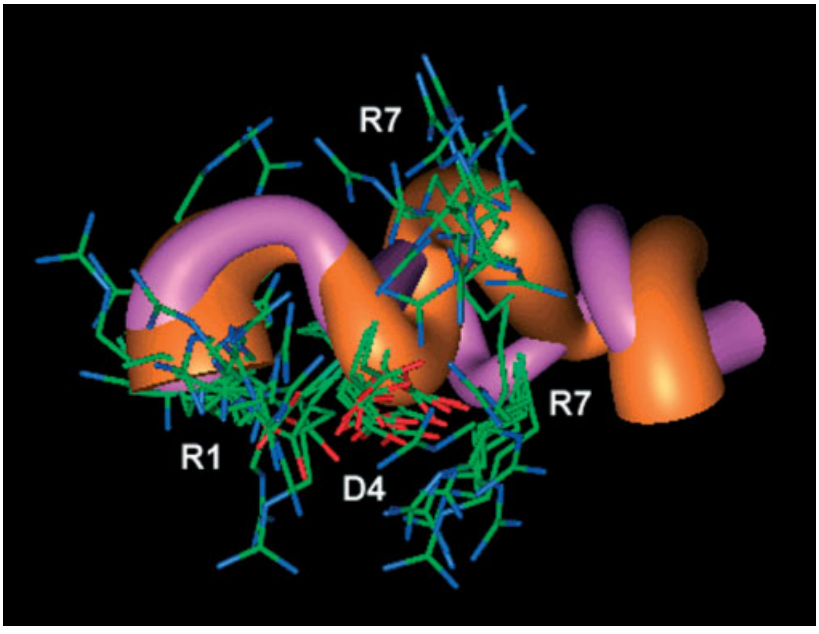

Figure 6 Overlay of the backbone atoms (segment 2–11) of the 20 best structures for analogue **4**. The two clusters are represented as cylinders of variable radius according to RMSD from the mean structure. The orientations of the R1, D4 and R7 side chains are also depicted.

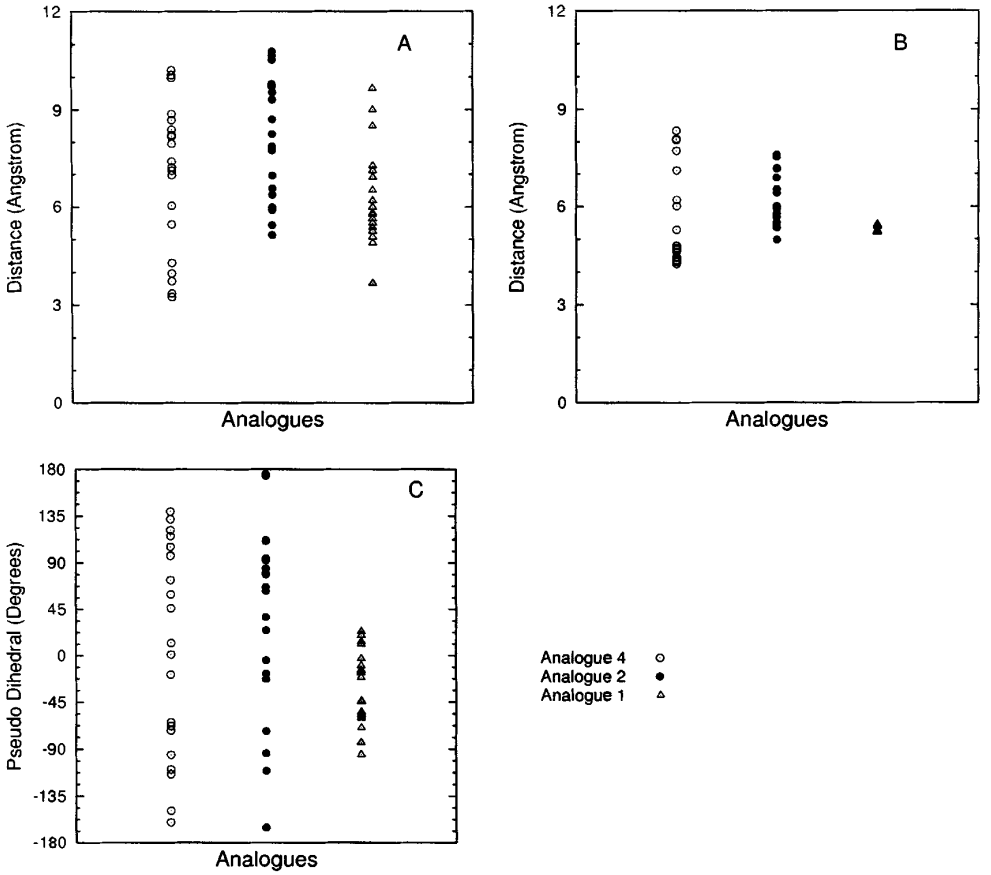

Figure 7 Distribution of the distance between R1(2) C^{ζ} and D4 C^{γ} (**A**); R1(2) C^{β} and D4 C^{β} (**B**); and the pseudo-dihedral angle (*pdo*) (**C**) for analogues **1**, **2** and **4**.

decided to apply the above three criteria to compounds (S,S) Ac-RCDCR-NH_2 ($IC_{50} = 4.3$ μM), (S,S) PRCDCK-NH_2 ($IC_{50} = 10.6$ μM), (S,S) Ac-RCDC-NH_2 ($IC_{50} = 105$ μM), Ac-SRGDVGRAibG K(Ac)AibG-OH (**1**) ($IC_{50} = 219$ μM), Ac-RGD-NH_2 ($IC_{50} \approx 500$ μM), Ac-SRGDVGNleAibGK(Ac)AibG-OH (**2**) ($IC_{50} \approx 2000$ μM) and Ac-RAibGDAibGRAibGK(Ac)AibG-OH (**4**) ($IC_{50} > 2000$ μM) which cover a wide range of inhibitory potency [55]. Figure 8A shows the distribution of the distance between the opposite charged centres for the 20 best structures of the seven analogues. It is clear that a good correlation can be established between the distance of the charged centres and the inhibitory potency of the analogues. As this distance increases, the biological activity also increases. Average values for this distance greater than 9.9 Å have been proposed for biologically active compounds [35,58,70]. The range of the distance of our active analogues falls within 4.3 (Ac-RGD-NH_2) to 10 Å ((S,S) Ac-RCDCR-NH_2). However, in the case of analogue **2**, which also falls within this range but it is inactive, this correlation cannot stand as a unique criterion. The same also holds true if the distance between the R C^{β} and D C^{β} atoms, which varies from 4.5 to 9 Å is correlated (Figure 8B).

The *pdo* value, as a structure–activity criterion, gives more accurate information, as it is evident from Figure 8C. Thus, as the *pdo* values converge to $-45^{\circ} \leq pdo \leq +45^{\circ}$, the anti-aggregatory activity increases. The inactive compounds have *pdo* values that strongly deviate ($-180^{\circ} \leq pdo \leq +180^{\circ}$) from the target angle interval (Figure 7C). It must be noted that despite the different computational methods [55,59] used for evaluating the structures of the presented analogues, the *pdo* criterion correlates very well with the activity of the compounds. Consequently, in order to achieve an enhanced activity, the positive and negative charge centres must be oriented toward the same side of the molecule. Overall, from the above results it is concluded that the fulfilment of the *pdo* criterion is a key requirement for a compound to exhibit inhibitory activity. Once this

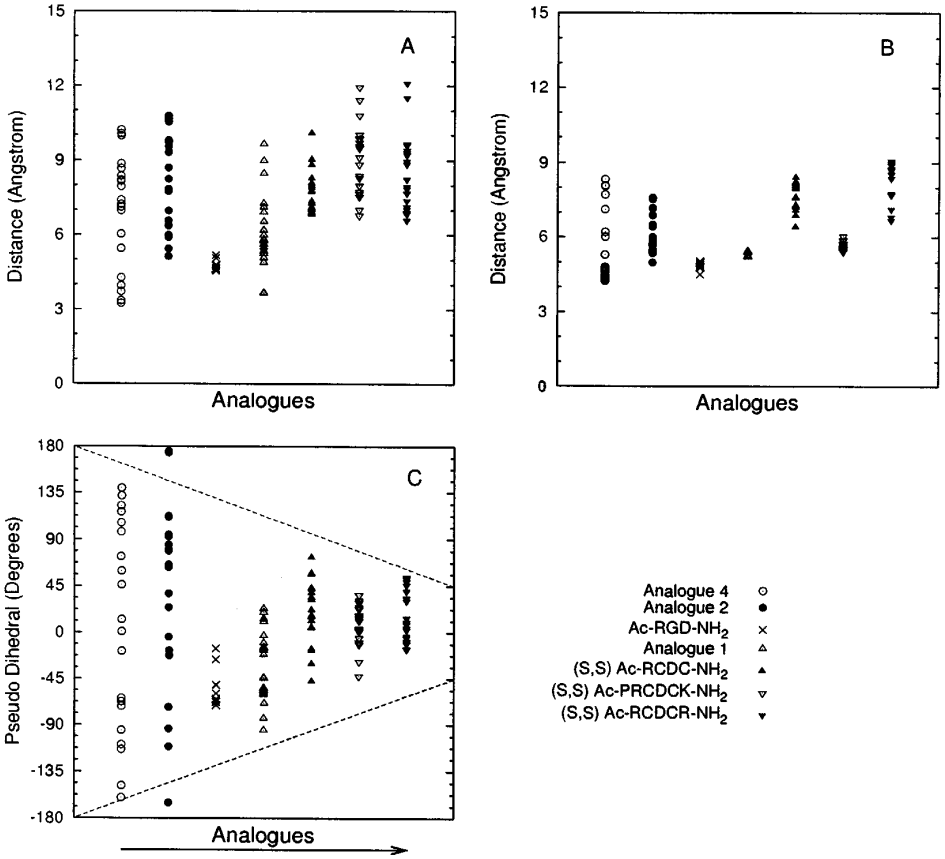

Figure 8 Distribution of the distance between R1(2) C^{ζ} and D4 C^{γ} (**A**); R1(2) C^{β} and D4 C^{β} (**B**); and the pseudo-dihedral angle (*pdo*) (**C**) for analogues **1**, **2**, **4**, (S,S) Ac-RCDCR-NH_2, (S,S) PRCDCK-NH_2, (S,S) Ac-RCDC-NH_2, and Ac-RGD-NH_2. From left to right (→) the anti-aggregatory activity of the corresponding analogue increases.

criterion is achieved, then the higher the distance between the charged centres and/or between the R and D C^{β} atoms, the better is the biological activity.

An ionic interaction between Arg and Asp side chains was not proposed for the (S,S) cyclic compounds [55], while it seems to stabilize the structure of Ac-RGD-NH_2 [59] and analogues **1** and **2**. In the case of analogue **1** this interaction was estimated to be weaker, compared with either Ac-RGD-NH_2 or analogue **2**. Interestingly, analogue **1** is the most active among them. It seems that the stronger the ionic interaction, the lower the anti-aggregatory activity (compare Ac-RGD-NH_2, analogue **1** and analogue **2**).

The enhancement of the biological activity induced by the presence of a second positive charge could be correlated either to conformational changes (compare the *pdo* values of **1** and **2**; Figure 7C) or to its direct involvement in integrin–ligand interaction. The orientation of the second positive charge, compared with the first Arg side chain (pseudo-dihedral angle defined by the R2 (R1) C^{ζ}, R2 (R1) C^{α}, R7 C^{α}, R7 C^{ζ} atoms) ranges from -45° to -180°, thus suggesting that they tend to adopt opposite orientations.

CONCLUSION

The target of this study was to estimate the validity of the criteria used for the evaluation of the structure–activity relationship of the RGD–containing peptides that could be the basis for the development of new, potent and specific RGD inhibitors.

The conformational analysis of the analogues **1–4**, revealed that, although the molecules contain residues (Aib) which can induce specific secondary conformational features [72], the local conformation of the RGD sequence in DMSO-d_6 solution is directed by the nature of the interaction between the opposite charged groups of the Arg and Asp

side chains. The strength of this interaction is greatly influenced by the residues flanking the RGD sequence. The criteria: (i) distance between the opposite charged centres, (ii) distance between the R and D C^{β} atoms, and (iii) pseudo-dihedral angle, *pdo*, defined by the R C^{ζ}, R C^{α}, D C^{α}, and D C^{γ} atoms were applied to seven RGD analogues and their correlation with the anti-aggregatory activity was estimated. It was found that neither the first, nor the second criterion could be applied separately for the discrimination between active and non active compounds. On the other hand, the $-45^{\circ} \leq pdo \leq +45^{\circ}$ criterion is sufficient to characterize the activity of an RGD analogue. However, the fulfilment of the *pdo* criterion, combined with the longer distances between the charged centres and/or between the R and D C^{β} atoms, are characteristic of the most potent inhibitors. It is also concluded that the occurrence and the strength of the ionic interaction between the Arg and Asp side chains are responsible for the decrease of the inhibitory potency of the RGD analogues.

Acknowledgements

The authors thank the European Union and the Ministry of National Education and Religious Affairs for financial support.

REFERENCES

1. Hynes RO. Integrins: a family of cell surface receptors. *Cell* 1987; **48**: 549–554.
2. Hynes RO. Integrins: versatility, modulation, and signaling in cell adhesion. *Cell* 1992; **69**: 11–25.
3. Ruoslahti E. RGD and other recognition sequences for integrins. *Annu. Rev. Cell. Dev. Biol.* 1996; **12**: 697–715.
4. Ruoslahti E, Pierschbacher MD. New perspectives in cell adhesion: RGD and integrins. *Science* 1987; **238**: 491–497.
5. Pierschbacher MD, Ruoslahti E. Influence of stereochemistry of the sequence Arg-Gly-Asp-Xaa on binding specificity in cell adhesion. *J. Biol. Chem.* 1987; **262**: 17 294–17 298.
6. Plow EF, Haas TA, Zhang L, Loftus J, Smith JW. Ligand binding to integrins. *J. Biol. Chem.* 2000; **275**: 21 785–21 788.
7. Torshin IY. Structural criteria of biologically active RGD-sites for analysis of protein cellular function: a bioinformatics study. *Med. Sci. Monit.* 2002; **8**: 301–312.
8. Gould RJ, Polokof MA, Friedman PA, Huang TF, Holt JC, Cook JJ, Niewiarowski S. Disintegrin: a family of integrin inhibitory proteins from viper venoms. *Proc. Soc. Exp. Biol. Med.* 1990; **195**: 168–171.
9. Ginsberg M, Pierschbacher MD, Ruoslahti E, Marguerie G, Plow E. Inhibition of fibronectin binding to platelets by proteolytic fragments and synthetic peptides which support fibroblast adhesion. *J. Biol. Chem.* 1985; **260**: 3931–3936.
10. Nicosia RF, Bonanno E. Inhibition of angiogenesis *in vitro* by Arg-Gly-Asp containing synthetic peptide. *Am. J. Pathol.* 1991; **138**: 829–833.
11. Bronson RA, Fusi F. Evidence that an Arg-Gly-Asp adhesion sequence plays a role in mammalian fertilization. *Biol. Reprod.* 1990; **43**: 1019–1025.
12. Ruggeri ZM. Receptor-specific antiplatelet therapy. *Circulation* 1989; **80**: 1920–1922.
13. Phillips DR, Charo IF, Scarborough RM. GPIIb-IIIa: the responsive integrin. *Cell* 1991; **65**: 359–362.
14. Kloczewiak M, Timmons S, Bednarek MA, Sakon M, Hawiger J. Platelet receptor recognition domain on the γ-chain of human fibrinogen and its synthetic peptide analogues. *Biochemistry* 1989; **28**: 2915–2919.
15. Haverstick DM, Cowan JF, Yamada KM, Santoro SA. Inhibition of platelet adhesion to fibronectin, fibrinogen, and von Willebrand factor substrates by a synthetic tetrapeptide derived from the cell-binding domain of fibronectin. *Blood* 1985; **66**: 946–952.
16. Plow EF, McEver BS, Coller BS, Woods VL, Marguerie GA, Ginsberg MH. Related binding mechanisms for fibrinogen, fibronectin, von Willebrand factor, and thrombospondin on thrombin-stimulated human platelets. *Blood* 1985; **66**: 724–727.
17. Pytela RP, Pierschbacher MD, Ginsberg MH, Plow EF, Ruoslahti E. Platelet membrane glycoprotein IIb/IIIa: member of a family of Arg-Gly-Asp specific adhesion receptors. *Science* 1986; **231**: 1559–1562.
18. Ruggeri ZM, De Marco L, Gatti L, Bader R, Montgomery RR. Platelets have more than one binding site for von Willebrand factor. *J. Clin. Invest.* 1983; **72**: 1–12.
19. Marguerie GA, Plow EF, Edgington TS. Human platelets possess an inducible and saturable receptor specific for fibrinogen. *J. Biol. Chem.* 1979; **254**: 5357–5363.
20. Sims PJ, Ginsberg MH, Plow EF, Shattil SJ. Effect of platelet activation on the conformation of the plasma membrane glycoprotein IIb-IIIa complex. *J. Biol. Chem.* 1991; **266**: 7345–7352.
21. Mayo KH, Fan F, Beavers MP, Eckardt A, Keane P, Hoekstra WJ, Andrade-Gordon P. RGD induces conformational transition in purified platelet integrin GPIIb/IIIa-SDS system yielding multiple binding states for fibrinogen γ-chain *C*-terminal peptide. *FEBS Lett.* 1996; **378**: 79–82.
22. Yan B, Hu DD, Knowles SK, Smith JW. Probing chemical and conformational differences in the resting

and active conformers of platelet integrin $\alpha_{IIb}\beta_3$. *J. Biol. Chem.* 2000; **275**: 7249–7260.
23. Ojima I, Chakravarty S, Dong Q. Antithrombotic agents: from RGD to peptide mimetics. *Bioorg. Med. Chem.* 1995; **3**: 337–360.
24. Pfaff M, Tangemann K, Muller B, Gurrath M, Muller G, Kessler H, Timpl R, Engel J. Selective recognition of cyclic RGD peptides of NMR defined conformation by αIIbβ3, αVβ3, and $\alpha 5\beta$1 integrins. *J. Biol. Chem.* 1994; **269**: 20 233–20 238.
25. Saudek V, Atkinson RA, Pelton JT. Three-dimensional structure of echistatin, the smallest active RGD protein. *Biochemistry* 1991; **30**: 7369–7372.
26. Chen Y, Pitzenberger SM, Garsky VM, Lumma PK, Sanyal G, Baum J. Proton NMR assignments and secondary structure of the snake venom protein echistatin. *Biochemistry* 1991; **30**: 11 625–11 636.
27. Atkinson RA, Saudek V, Pelton JT. Echistatin: the refined structure of a disintegrin in solution by ^{1}H NMR and restrained molecular dynamics. *Int. J. Pept. Protein Res.* 1994; **43**: 563–572.
28. Adler M, Lazarus RA, Dennis MS, Wagner G. Solution structure of kistrin, a potent platelet aggregation inhibitor and GP IIb-IIIa antagonist. *Science* 1991; **253**: 445–448.
29. Adler M, Wagner G. Sequential ^{1}H NMR assignments of kistrin, a potent platelet aggregation inhibitor and glycoprotein IIb-IIIa antagonist. *Biochemistry* 1992; **3**: 1031–1039.
30. McDowell RS, Dennis MS, Louie A, Shuster M, Mulkerrin MG, Lazarus RA. Mambin, a potent glycoprotein IIb-IIIa antagonist and platelet aggregation inhibitor structurally related to the short neurotoxins. *Biochemistry* 1992; **31**: 4766–4772.
31. Senn H, Klaus W. The nuclear magnetic resonance solution structure of flavoridin, an antagonist of the platelet GP IIb-IIIa receptor. *J. Mol. Biol.* 1993; **232**: 907–925.
32. Jaseja M, Lu X, Williams JA, Sutcliffe MJ, Kakkar VV, Parslow RA, Hyde EI. ^{1}H NMR assignments and secondary structure of dendroaspin, an RGD-containing glycoprotein IIb-IIIa (αIIb-β3) antagonist with a neurotoxin fold. *Eur. J. Biochem.* 1994; **226**: 861–868.
33. Krezel AM, Wagner G, Seymour-Ulmer J, Lazarus RA. Structure of the RGD protein decorsin: conserved motif and distinct function in leech proteins that affect blood clotting. *Science* 1994; **264**: 1944–1947.
34. Smith KJ, Jaseja M, Lu X, Williams JA, Hyde EI, Trayer IP. Three-dimensional structure of the RGD-containing snake toxin albolabrin in solution, based on ^{1}H NMR spectroscopy and simulated annealing calculations. *Int. J. Pept. Protein Res.* 1996; **48**: 220–228.
35. Krezel AM, Ulmer JS, Wagner G, Lazarus RA. Recombinant decorsin: dynamics of the RGD recognition site. *Protein Sci.* 2000; **9**: 1428–1438.
36. Samanen J, Ali F, Romoff T, Calvo R, Sorenson E, Vasko J, Storer B, Berry D, Bennett D, Strohsacker M, Powers D, Stadel J, Nichols A. Development of a small RGD peptide fibrinogen receptor antagonist with potent antiaggregatory activity *in vitro*. *J. Med. Chem.* 1991; **34**: 3114–3125.
37. Yamada KM. Adhesive recognition sequences. *J. Biol. Chem.* 1991; **266**: 12 809–12 812.
38. Hynes RA, Lander AD. Contact and adhesive specificities in the associations, migrations, and targeting of cells and axons. *Cell* 1992; **68**: 303–322.
39. D'Souza SE, Ginsberg M, Plow EF. Arginyl-glycyl-aspartic acid (RGD): a cell adhesion motif. *Trends Biochem. Sci.* 1991; **16**: 246–250.
40. Lanza P, Felding-Habermann B, Ruggeri ZM, Zanetti M, Billetta R. Selective interaction of a conformationally-constrained Arg-Gly-Asp (RGD) motif with the integrin receptor αvβ3 expressed on human tumor cells. *Blood Cells Mol. Dis.* 1997; **23**: 230–241.
41. Mayo KH, Fan F, Beavers MP, Eckardt A, Keane P, Hoekstra WJ, Andrade-Gordon P. NOE-derived conformation of GRGDSP cell adhesion recognition site in the presence of SDS micelles and integrin receptor GPIIB/IIIA. *Biochim. Biophys. Acta* 1996; **1296**: 95–102.
42. Aumailley M, Gurrath M, Muller G, Calvete J, Timpl R, Kessler H. Arg-Gly-Asp constrained within cyclic pentapeptides. Strong and selective inhibitors of cell adhesion to vitronectin and laminin fragment P1. *FEBS Lett.* 1991; **291**: 50–54.
43. Bach AC, Eyermann CJ, Gross JD, Bower MJ, Harlow RL, Weber PC, DeGrado WF. Structural studies of a family of high affinity ligands for GPIIb/IIIa. *J. Am. Chem. Soc.* 1994; **116**: 3207–3219.
44. Mer G, Kellenberger E, Lefevre J-F. α-Helix mimicry of a β-turn. *J. Mol. Biol.* 1998; **281**: 235–240.
45. McDowell RS, Blackburn BK, Gadek TR, McGee LR, Rawson T, Reynolds ME, Robarge KD, Somers TC, Thorsett ED, Tischler M, Webb RR, Venuti MC. From peptide to non-peptide 2. The *de novo* design of potent, non-peptidal inhibitors of platelet aggregation based on a benzodiazepinedione scaffold. *J. Am. Chem. Soc.* 1994; **116**: 5077–5083.
46. Johnson WC, Pagano TG, Basson CT, Madri JA, Gooley P, Armitage IM. Biologically active Arg-Gly-Asp oligopeptides assume a type II β-turn in solution. *Biochemistry* 1993; **32**: 268–273.
47. Haubner R, Gratias R, Diefenbach B, Goodman SL, Jonczyk A, Kessler H. Structural and functional aspects of RGD-containing cyclic pentapeptides as highly potent and selective integrin $\alpha_v\beta_3$ antagonists. *J. Am. Chem. Soc.* 1996; **118**: 7461–7472.
48. Bach AC, Espina JR, Jackson SA, Stouten PFW, Duke JL, Mousa SA, DeGrado WF. Type II′ to type I β-turn swap changes specificity for integrins. *J. Am. Chem. Soc.* 1996; **118**: 293–294.
49. Assa-Munt N, Jia X, Laakkonen P, Ruoslahti E. Solution structures and integrin binding activities of

an RGD peptide with two isomers. *Biochemistry* 2001; **40**: 2373–2378.
50. Dechantsreiter MA, Planker E, Matha B, Lohof E, Holzemann G, Jonczyk A, Goodman SL, Kessler H. *N*-Methylated cyclic RGD peptides as highly active and selective $\alpha_v\beta_3$ integrin antagonists. *J. Med. Chem.* 1999; **42**: 3033–3040.
51. Miyashita M, Akamatsu M, Hayashi Y, Ueno T. Three-dimensional quantitative structure-activity relationship analyses of RGD mimetics as fibrinogen receptor antagonists. *Bioorg. Med. Chem. Lett.* 2000; **10**: 859–863.
52. Craig WS, Cheng S, Mullen D, Blevitt J, Pierschbacher MD. Concept and progress in the development of RGD-containing peptide pharmaceuticals. *Biopolymers* 1995; **37**: 157–175.
53. Lu X, Sun Y, Shang D, Wattam B, Egglezou S, Hughes T, Hyde E, Scully M, Kakkar V. Evaluation of the role of proline residues flanking the RGD motif of dendroaspin, an inhibitor of platelet aggregation and cell adhesion. *Biochem. J.* 2001; **355**: 633–638.
54. Zachariah C, Cameron A, Lindberg I, Kao KJ, Beinfeld MC, Edison AS. Structural studies of a neuropeptide precursor protein with an RGD proteolytic site. *Biochemistry* 2001; **40**: 8790–8799.
55. Stavrakoudis A, Bizos G, Eleftheriadis D, Kouki A, Panou-Pomonis E, Sakarellos-Daitsiotis M, Sakarellos C, Tsoukatos D, Tsikaris V. A three-residue cyclic scaffold of non-RGD containing peptide analogues as platelet aggregation inhibitors: design, synthesis, and structure-function relationships. *Biopolymers* 2001; **56**: 20–26.
56. Stavrakoudis A, Tsoukatos D, Sakarellos-Daitsiotis M, Sakarellos C, Tsikaris V. Studies on the structure-function relationships of cyclic non-RGD peptides. In *Peptides 2000*, Martinez J, Fehrentz JA. (eds). EDK: Paris, 2001; 439–440.
57. Stote RH. Analysis of the RGD sequence in protein structures: a comparison to the conformations of the RGDW and $_D$RGDW peptides determined by molecular dynamics simulations. *Theor. Chem. Acc.* 2001; **106**: 128–136.
58. Bartels C, Stote RH, Karplus M. Characterization of flexible molecules in solution: the RGDW peptide. *J. Mol. Biol.* 1998; **284**: 1641–1660.
59. Biris N, Stavrakoudis A, Politou AS, Mikros E, Sakarellos-Daitsiotis M, Sakarellos C, Tsikaris V. The Ac-RGD-NH_2 peptide as a probe of slow conformational exchange of short linear peptides in DMSO. *Biopolymers* 2003; **69**: 72–86.
60. Tsikaris V, Sakarellos C, Sakarellos-Daitsiotis M, Orlewski P, Marraud M, Cung MT, Vatzaki E, Tzartos S. Construction and application of a new class of sequential oligopeptide carriers (SOC_n) for multiple anchoring of antigenic peptides: application to the acetylcholine receptor (AChR) main immunogenic region. *Int. J. Biol. Macromol.* 1996; **19**: 195–205.
61. Tsikaris V, Sakarellos C, Cung MT, Marraud M, Sakarellos-Daitsiotis M. Concept and design of a new class of sequential oligopeptide carriers (SOC) for covalent attachment of multiple antigenic peptides. *Biopolymers* 1996; **38**: 291–293.
62. Stewart JM, Young JD (eds). *Solid Phase Peptide Synthesis*. Pierce Chem. Co.: Rockford, IL, 1984; 71–95.
63. Güntert P, Mumenthaler C, Wüthrich K. Torsion angle dynamics for NMR structure calculation with the new program DYANA. *J. Mol. Biol.* 1997; **273**: 283–298.
64. Wüthrich K, Billeter M, Braun W. Pseudo-structures for the 20 common amino acids for use in studies of protein conformations by measurements of intramolecular proton–proton distance constraints with nuclear magnetic resonance. *J. Mol. Biol.* 1983; **169**: 949–961.
65. Koradi R, Billeter M, Wüthrich K. MOLMOL: a program for display and analysis of macromolecular structures. *J. Mol. Graph.* 1996; **14**: 51–55.
66. Tsikaris V, Cung MT, Panou-Pomonis E, Sakarellos C, Sakarellos-Daitsiotis M. ^{1}H NMR studies on the preferred interactions of guanidinium and *C*-terminal carboxylate groups in arginine containing peptides. *J. Chem. Soc., Perkin Trans. 2* 1993; 1345–1349.
67. Tsikaris V, Sakarellos-Daitsiotis M, Tzovaras D, Sakarellos C, Orlewski P, Cung MT, Marraud M. Isomerization of the Xaa-Pro peptide bond induced by ionic interactions of arginine. *Biopolymers* 1996; **38**: 672–673.
68. Benedetti E, Morelli G, Némethy G, Scheraga HA. Statistical and energetic analysis of side-chain conformations in oligopeptides. *Int. J. Pept. Protein Res.* 1983; **22**: 1–15.
69. McGregor MJ, Islam SA, Sternberg MJ. Analysis of the relationship between side-chain conformation and secondary structure in globular proteins. *J. Mol. Biol.* 1987; **198**: 295–310.
70. Jackson S, DeGrado W, Dwivedi A, Parthasarathy A, Higley A, Krywko J, Rockwell A, Markwalder J, Wells G, Wexler R, Mousa S, Harlow R. Template-constrained cyclic peptides: design of high-affinity ligands for GPIIb/IIIa. *J. Am. Chem. Soc.* 1994; **116**: 3220–3230.
71. Markley JL, Bax A, Arata Y, Hilbers W, Kaptein R, Sykes BD, Wright PE, Wüthrich K. Recommendations for the presentation of NMR structures of proteins and nucleic acids. *Pure Appl. Chem.* 1998; **70**: 117–142.
72. Toniolo C, Crisma M, Formaggio F, Peggiom C. Control of peptide conformation by the Thorpe-Ingold effect (C^α-tetrasubstitution). *Biopolymers (Pept. Sci.)* 2001; **60**: 396–419.

